Broad Band-Pass and Band-Stop Transmissions Through the Hybrid Gratings of Rectangle and Triangle

Xiaojun Tian, Yongkai Wang, Liang Cao, and Zhongyue Zhang

***Abstract*—Silver gratings of hybrid structures are proposed, and their optical transmission properties are simulated by finite element method. The proposed structure is found to facilitate a broadband-enhanced transmission in the infrared region and exerts a band-stop effect in the visible region. The effects of structural parameters on transmission characteristics are also studied. Results reveal promising applications in broadband light harvesting and filtering devices.**

***Index Terms*—Extraordinary optical transmission, finite element method, localized surface plasmon, surface plasmon polaritons.**

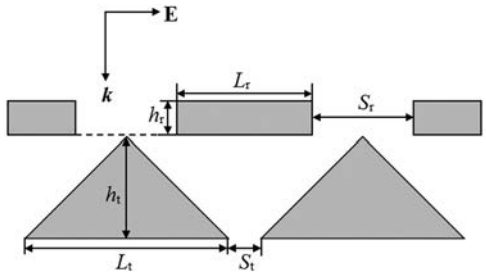

Fig. 1. The proposed hybrid gratings and their structural parameters.

I. Introduction

THE extraordinary optical transmission (EOT) phenomenon was first demonstrated in 1998 in an opaque metallic film perforated by a periodic array of sub-wavelength holes [1]. The transmittances at specific wavelengths were several orders of magnitudes larger than the percentage of the overall area covered with holes. In addition to the efficient power funneling of the electromagnetic fields, EOT also offers strong field confinement and enhancement with potential applications in sub-wavelength integrated optics [2] and sensors [3], [4].

Extensive investigations have conducted to explore the underlying physical mechanisms of the EOT phenomenon and to tune the structural features of sub-wavelength hole structures for higher transmission [5]–[24]. One theory called Wood's anomaly or Rayleigh anomaly has been demonstrated, which is based on an expansion of the scattered electromagnetic field; it only occurs at specific wavelengths where a new diffracted order emerges from the grating at the grazing angle [5], [6]. In addition, researchers have found that the coupling between incident light and metal surface plasmon polaritons (SPPs) also plays an important role in EOT [7]. When the reciprocal lattice vector of the hole array period matches the SPP momentum, the electric field around the hole aperture is highly enhanced and contributes to the funneling of light through the structure. The localized surface plasmon (LSP) resonance in the hole apertures is also important in EOT [8]–[11]. For example, an array of holes with acute angles indicates a strong EOT effect caused by LSP [11]. Ruan *et al*. also found that the localized waveguide resonance in holes results in EOT, and the hole can be regarded as a section of metallic waveguide with both ends open to free space [12].

The said mechanisms result in the resonant EOT phenomenon with a narrow spectral bandwidth [13]–[15]. Furthermore, the broadband transparency is also valuable and can be realized using a non-resonant approach, such as oblique incidence TM polarization [16], [17], connection between larger rectangular apertures and smaller apertures [18], or metallic gratings with tapered slits [19].

Hybrid structures may produce interesting transmission properties [25], [26]. This study indicates that the hybrid gratings of rectangle and triangle can generate broadband transparency under normal incidence for TM polarized light. The finite element method is used to analyze numerically the transmission characteristics of the gratings. Results reveal that the proposed structure achieves broad band-pass and band-stop transmissions in the infrared and visible region, respectively. The effects of structural parameters on the transmission properties have also been investigated. These results can help in near-field light harvesting and filtering applications.

II. Structure and Computational Methods

Fig. 1 shows two unit cells of the silver-hybrid gratings that comprise rectangle and triangle gratings. The rectangle grating is characterized by length L_{r}, thickness h_{r}, and separation S_{r}. The corresponding parameters of the triangle grating are L_{t}, h_{t}, and S_{t}, respectively. The values of h_{r} and h_{t} are fixed at 20 and 60 nm, respectively, in our calculation. The entire

Manuscript received December 16, 2014; revised June 11, 2015, August 7, 2015, and October 25, 2015; accepted November 30, 2015. Date of publication December 10, 2015; date of current version February 10, 2016. This work was supported by the National Science Foundation of China under Grant 11004160, the Fundamental Research Funds for the Central Universities under Grant GK201303007, and the Funds for Undergraduate Students Innovation Training (201310718035).

The authors are with the School of Physics and Information Technology, Shaanxi Normal University, Xi'an 710062, China (e-mail: zyzhang@snnu.edu.cn; wang_yong_kai@126.com; caolianger2011@gmail.com; zyzhang@snnu.edu.cn).

Color versions of one or more of the figures in this paper are available online at http://ieeexplore.ieee.org.

Digital Object Identifier 10.1109/JLT.2015.2506343

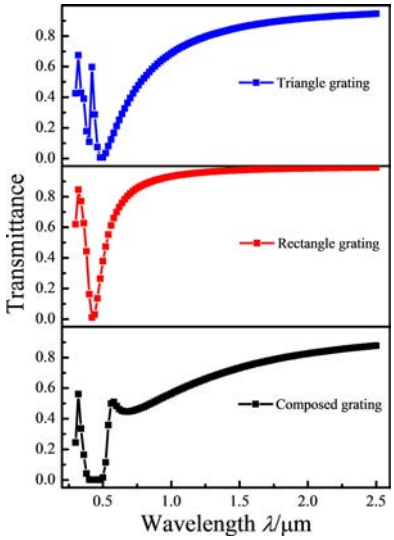

Fig. 2. Transmission spectra of the hybrid grating, the rectangle grating, and triangle grating.

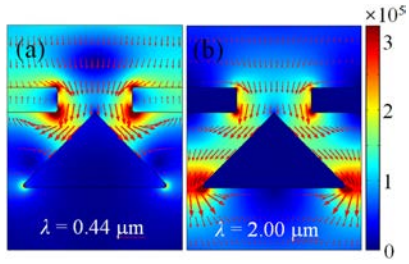

Fig. 3. Distribution of the electric fields and energy flows at different wavelengths: (a) $\lambda = 0.44\ \mu$m; (b) $\lambda = 2.00\ \mu$m.

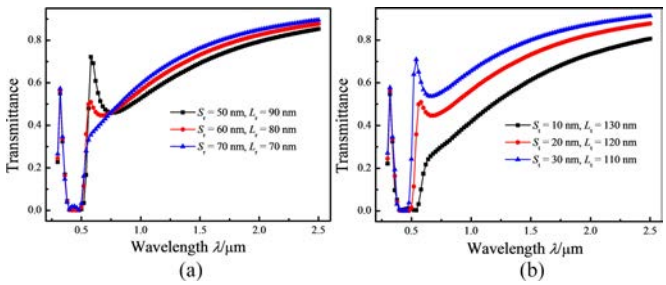

Fig. 4. Transmission spectra of the hybrid gratings with different separations: (a) different S_r; (b) different S_t.

structure is periodic in the horizontal direction and satisfies $L_r + S_r = L_t + S_t$. The transmission coefficients and electric field distributions are simulated using a commercial finite element method software (COMSOL Multiphysics). The transmission coefficient is defined as the rate of output power P_{out} to input power P_{in}, namely, $T = P_{out}/P_{in}$. The frequency-dependent complex relative permittivities of silver are referred to in [27]. The incident light propagates along the vertical direction with the polarization in the horizontal direction in all calculations.

III. Results and Discussion

Fig. 2 shows the transmission spectra of the hybrid and rectangle gratings for the wavelength that ranges from 0.3 to 2.5 μm. The structural parameter values are $L_r = 80$ nm, $L_t = 120$ nm, $S_r = 60$ nm, and $S_t = 20$ nm. Fig. 2 shows that a broad band-stop appears in the visible region (0.4 to 0.5 μm), and a broad band-pass (At $\lambda = 2.5\ \mu$m, the transmittance is 0.88. It can be even larger if the wavelength is longer than 2.5 μm, and reaches 0.96 at $\lambda = 5.00\ \mu$m.) appears in the infrared region in the transmission spectrum of the hybrid gratings. At the same time, the reflection spectrum (not shown in this paper) reveals high reflectance in the visible region. We also calculated the transmission spectrum of the rectangle grating with the same structural parameters as those in the hybrid gratings, as the red line shows in Fig. 2. A single valley appears at $\lambda = 0.42\ \mu$m, which is due to the LSP resonance on the rectangle. In the transmission spectrum (blue line) of the triangle grating, two valleys of appear at $\lambda = 390$ nm and $\lambda = 490$ nm, which are due to LSPR of triangle gratings, respectively. When the triangle gratings is designed under the rectangle gratings, the valley around $\lambda = 0.42\ \mu$m forms a broad band-stop region. In Fig. 1, the band-stop width of the hybrid grating increases to 260 nm comparing with 200 nm of rectangle grating and 140 nm of triangle grating. The electric field and energy flow distributions at both regions were calculated to understand the mechanisms in Fig. 2. When the excitation wavelength is 0.44 μm (i.e., a representative wavelength in the band-stop region) as shown in Fig. 3(a), a strong electric field is mainly distributed around the rectangle and most of the energy is scattered. This band-stop region is mainly due to the LSP of the rectangle, which is affected by the triangle in the hybrid gratings. The oblique plane of the triangle causes continuously different coupling distances between the rectangle and triangle, which results in a broad band-stop region in the transmission spectrum. At the wavelength of 2.00 μm (i.e., a representative wavelength in the band-pass region), the electric fields are mainly distributed at the ends of the rectangle and bottom tips of the triangle, as shown in Fig. 3(b). The energy flows along the hypotenuses of the triangle. Adjacent triangles form tapered slits, and the energy flows from the entrance at the top to the exit at the bottom. The energy is coupled from the rectangle to the tapered slits at the entrance, and then propagates to the narrow exit of the tapered grating, which has a similar mechanism as that in [19]. When the wavelength of the incident light is much larger than the grating structure period, electrons in the metal congregate to the exit of the tapered grating. The formed strong electron oscillation field between the two sides of the narrow exit slit promotes enhanced optical transmission in the infrared region.

The dimensions of the hybrid gratings are varied systematically to investigate how the structural parameters affect the transmission spectra of the hybrid gratings. Fig. 4 shows the effect of different separation S_r and S_t values on the transmission spectra. The period is fixed at 140 nm. First, S_r is noted at 50, 60, and 70 nm (i.e., the corresponding values of L_r are 90, 80, and 70 nm, respectively) with fixed $L_t = 120$ nm and $S_t = 20$ nm. Fig. 4 (a) shows that the transmittances of the band-stop region do not vary clearly. The transmittances at the band-pass

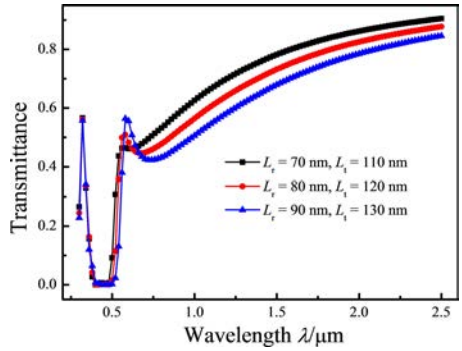

Fig. 5. Transmission spectra of the hybrid gratings with different L_{r} and L_{t} which are varied synchronously with fixed $S_{\mathrm{r}} = 60$ nm and $S_{\mathrm{t}} = 20$ nm.

region increase as S_{r} increases. Given that the band-stop region is due to the electric field coupling between the rectangle and triangle hypotenuses, S_{r} does not largely affect the electric field coupling and the transmission properties in the band-stop region is insensitive to the S_{r} variation. Moreover, the larger separation S_{r} indicates a larger entrance, which allows more energy to enter the tapered slits and pass through. This reason leads to the increasing transmission coefficient in the infrared region as S_{r} increases. At the transmission peak of 0.58 μm for $S_{\mathrm{r}} = 50$ nm, maximum electric fields distribute around the tips of the rectangle and bottom tips of the triangle. The tapered slits work as a Fabry–Perot resonator. A smaller S_{r} indicates larger reflectance at the entrance of the tapered slits, which results in stronger transmittance at the exit of the tapered slits.

Similarly, the effect of triangle separation S_{t} is also investigated by taking its values at 10, 20, and 30 nm (i.e., the corresponding values of L_{t} are 130, 120, and 110 nm, respectively) with fixed $L_{\mathrm{r}} = 80$ nm and $S_{\mathrm{r}} = 60$ nm, as shown in Fig. 4(b). The broad band-stop and band-pass regions occur in the transmission spectra for different S_{t} values. The band-stop width of the hybrid grating decreases from 320 to 220 nm and the transmittances in the infrared region increase as S_{t} increases. The shorter length of the triangle L_{t} results in a longer electric field coupling distance between the triangle and rectangle. The LSP wavelength also blue shifts. The increasing separation between two adjacent triangles leads to smaller impedance for SPPs that propagate through the tapered slits, which produces larger transmittance in the infrared region.

Furthermore, the effects of synchronous change of L_{r} and L_{t} on the transmission properties of the hybrid gratings are investigated by taking their L_{r} values at 70, 80, and 90 nm, as well as the corresponding L_{t} values of 110, 120, and 130 nm, respectively (see Fig. 5). In Fig. 5, the band-stop width of the hybrid grating increases from 240 to 280 nm with the increase of L_{r}. The separations of the rectangle and triangle gratings are fixed at $S_{\mathrm{r}} = 60$ nm and $S_{\mathrm{t}} = 20$ nm, respectively. Given that a longer L_{r} results in a longer electron oscillation distance, the bandwidth of the band-stop region increases to the longer wavelength. Moreover, the transmittances decrease in the band-pass region with the increase in L_{r} and L_{t}, which is due to the larger impedance for SPPs that propagate through the tapered slits.

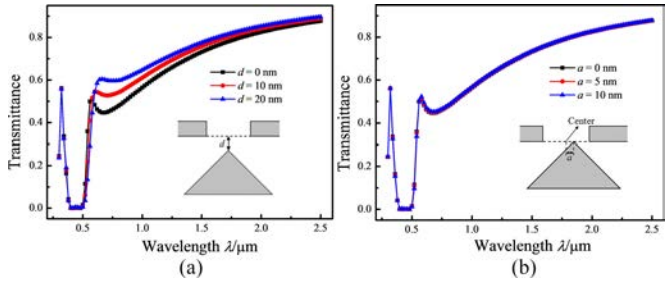

Fig. 6. Transmission spectra of the hybrid gratings with different vertical and horizontal relative displacements: (a) different vertical relative displacements; (b) different horizontal relative displacements.

In addition, the transmission spectra of the hybrid gratings with different vertical and horizontal relative displacements are calculated with a fixed $L_{\mathrm{r}} = 80$ nm, $L_{\mathrm{t}} = 120$ nm, $S_{\mathrm{r}} = 60$ nm, and $S_{\mathrm{t}} = 20$ nm to demonstrate the effect of relative positions of the two gratings on the said spectra. Fig. 6(a) shows the transmission spectra of the hybrid gratings with different vertical relative displacements (noted with *d*, which represents the distance between rectangle and triangle gratings). The larger *d* yields a higher transmission coefficient in the infrared region, because the larger entrance of the tapered slits allows more energy to enter the tapered slits. The transmittances and bandwidth of the band-stop region do not vary clearly. The effect of the relative horizontal displacements (noted with *a*, which represents the value of the triangles that deviate from the middle of adjacent rectangles) on the transmission spectra is presented in Fig. 6(b). The transmittances at the broad band-stop and band-pass regions do not clearly change. Broad band-stop is due to bonding coupling between rectangles and triangles. In Fig. 6(a), the slight red shift of broad band-stop is due to the increase of coupling distance in vertical direction with the increase of *d*. In Fig. 6(b), the broad band-stop region does not shift obviously, which is due to total coupling distance to left and right adjacent triangles is not change with the increase of *a*. The results in Fig. 6(a) and (b) reveal the transmittance robustness of the hybrid gratings to relative displacements between rectangles and triangles. This scenario offers much convenience to the fabrication of the hybrid gratings.

IV. Conclusion

This paper presents hybrid gratings made up of rectangle and triangle gratings. The transmission coefficients and electric field distributions of the hybrid gratings were analyzed numerically using the finite element method. Broadband-enhanced transmission in the infrared region and a broad band-stop effect in the visible region are observed in the transmittance spectra. The broad band-stop region is a result of the LSP in the hybrid gratings. The hybrid grating at the broad band-pass region works as tapered slits, and SPPs propagate along the triangle hypotenuses. Although the transmission spectra of the hybrid gratings are strongly dependent on the structural parameters of rectangles and triangles, the transmission spectra are robust to relative displacements between rectangles and triangles, which offers much convenience to the fabrication of the hybrid grat-

ings. These results can help in broadband light harvesting and filtering applications.

REFERENCES

[1] T. W. Ebbesen, H. J. Lezec, H. F. Ghaemi, T. Thio, and P. A. Wolff, "Extraordinary optical transmission through sub-wavelength hole arrays," *Nature*, vol. 391, no. 6668, pp. 667–669, Feb. 1998.

[2] H. Herrmann, K. D. Buchter, R. Ricken, and W. Sohler, "Tunable integrated electro-optic wavelength filter with programmable spectral response," *J. Lightw. Technol.*, vol. 28, no. 7, pp. 1051–1056, Jan. 2010.

[3] Y. Su, Y. Ke, S. Cai, and Q. Yao, "Surface plasmon resonance of layer-by-layer gold nanoparticles induced photoelectric current in environmentally-friendly plasmon-sensitized solar cell," *Light: Sci. Appl.*, vol. 1, no. e14, pp. 1–5, Jun. 2012.

[4] Y. Huang, Y. Fang, Z. Zhang, L. Zhu, and M. Sun, "Nanowire-supported plasmonic waveguide for remote excitation of surface-enhanced Raman scattering," *Light: Sci. Appl.*, vol. 3, no. E199, pp. 1–17, Aug. 2014.

[5] A. Hessel and A. A. Oliner, "A new theory of Wood's anomalies on optical gratings," *Appl. Opt.*, vol. 4, no. 10, pp. 1275–1297, Oct. 1965.

[6] N. Garcia and M. Nieto-Vesperinas, "Theory of electromagnetic wave transmission through metallic gratings of subwavelength slits," *J. Opt. A, Pure Appl. Opt.*, vol. 9, no. 5, pp. 490–495, May 2007.

[7] C. Genet, and T. W. Ebbesen, "Light in tiny holes," *Nature*, vol. 445, no. 7123, pp. 39–46, Jan. 2007.

[8] K. J. K. Koerkamp, S. Enoch, F. B. Segerink, N. F. V. Hulst, and L. Kuipers, "Strong influence of hole shape on extraordinary transmission through periodic arrays of subwavelength holes," *Phys. Rev. Lett.*, vol. 92, no. 18, pp. 1839011–1839014, May. 2004.

[9] R. Gordon, A. G. Brolo, A. McKinnon, A. Rajora, B. Leathem, and K. L. Kavanagh, "Strong polarization in the optical transmission through elliptical nanohole arrays," *Phys. Rev. Lett.*, vol. 92, no. 3, pp. 037401-1–037401-4, Jan. 2004.

[10] S. M. Orbons and A. Roberts, "Resonance and extraordinary transmission in annular aperture arrays," *Opt. Exp.*, vol. 14, no. 26, pp. 12623–12628, Dec. 2006.

[11] S. G. Rodrigo, O. Mahboub, A. Degiron, C. Genet, F. J. Garcia-Vidal, L. Martin-Moreno, and T. W. Ebbesen, "Holes with very acute angles: A new paradigm of extraordinary optical transmission through strongly localized modes," *Opt. Exp.*, vol. 18, no. 23, pp. 23691–23697, Nov. 2010.

[12] Z. C. Ruan and M. Qiu, "Enhanced transmission through periodic arrays of subwavelength holes: The role of localized waveguide resonances," *Phys. Rev. Lett.*, vol. 96, no. 23, pp. 233901-1–233901-4, Jun. 2006.

[13] R. Marani, V. Marrocco, M. Grande, G. Morea, A. D'Orazio, and V. Petruzzelli, "Enhancement of extraordinary optical transmission in a double heterostructure plasmonic bandgap cavity," *Plasmonics*, vol. 6, no. 3, pp. 469–476, Mar. 2011.

[14] Y. M. Hou, "Extremely high transmittance at visible wavelength induced by magnetic resonance," *Plasmonics*, vol. 6, no. 2, pp. 289–293, Jan. 2011.

[15] G. H. Rui, Q. W. Zhan, and H. Ming, "Nanoantenna-assisted extraordinary optical transmission under radial polarization illumination," *Plasmonics*, vol. 6, no. 3, pp. 521–525, Sep. 2011.

[16] X. R. Huang, R. W. Peng, and R. H. Fan, "Making metals transparent for white light by spoof surface plasmons," *Phys. Rev. Lett.*, vol. 105, no. 24, pp. 243901-1–243901-4, Dec. 2010.

[17] A. Alù, G. D'Aguanno, N. Mattiucci, and M. J. Bloemer, "Plasmonic Brewster angle: Broadband extraordinary transmission through optical gratings," *Phys. Rev. Lett.*, vol. 106, no. 12, pp. 123902-1–123902-4, Mar. 2011.

[18] G. Subramania, S. Foteinopoulou, and I. Brener, "Nonresonant broadband funneling of light via ultrasubwavelength channels," *Phys. Rev. Lett.*, vol. 107, no. 16, pp. 163902-1–163902-5, Oct. 2011.

[19] H. H. Shen and B. Maes, "Enhanced optical transmission through tapered metallic grating," *Appl. Phys. Lett.*, vol. 100, no. 24, pp. 241104–1–241104-3, Jun. 2012.

[20] Y. Wang, Y. Qin, and Z. Zhang, "Extraordinary optical transmission property of X-Shaped plasmonic nanohole arrays," *Plasmonics*, vol. 9, no. 2, pp. 203–207, Apr. 2014.

[21] R. D. Nevels and K. A. Michalski, "On the behavior of surface plasmons at a metallo-dielectric interface," *J. Lightw. Technol.*, vol. 32, no. 19, pp. 3299–3305, Oct. 2014.

[22] L. Chen, Y. Zhu, X. Zang, B. Cai, Z. Li, L. Xie, and S. Zhuang, "Mode splitting transmission effect of surface wave excitation through a metal hole array," *Light: Sci. Appl.*, vol. 2, no. e60, pp. 1–5, Mar. 2013.

[23] Y. J. Bao, R. W. Peng, D. J. Shu, M. Wang, X. Lu, J. Shao, W. Lu, and N. B. Ming, "Role of interference between localized and propagating surface waves on the extraordinary optical transmission through a subwavelength-aperture array," *Phys. Rev. Lett.*, vol. 101, no. 8, pp. 087401-1–087401-1, Aug. 2008.

[24] Y. Ding, J. Yoon, M. H. Javed, S. H. Song, and R. Magnusson, "Mapping surface-plasmon polaritons and cavity modes in extraordinary optical transmission," *IEEE Photon. J.*, vol. 3, no. 3, pp. 365–374, Jun. 2011.

[25] H. Liu, B. Li, L. Zheng, C. Xu, G. Zhang, X. Wu, and N. Xiang, "Multispectral plasmon-induced transparency in triangle and nanorod(s) hybrid nanostructures," *Opt. Lett.*, vol. 38, no. 6, pp. 977–979, Mar. 2013.

[26] H. Lochbihler and Y. Ye, "Two-dimensional subwavelength gratings with different frontside/backside reflectance," *Opt. Lett.*, vol. 38, no. 7, pp. 1028–1030, Apr. 2013.

[27] P. B. Johnson and R. W. Christy, "Optical constants of the noble metals," *Phys. Rev. B*, vol. 6, no. 12, pp. 4370—4379, Jul. 1972.

Xiaojun Tian is a B.S. student in Shaanxi Normal University. She interests in plasmonics.

Yongkai Wang received his M.S. degree of optical engineering in 2015 from Shaanxi Normal University. Currently, he is a Ph.D. candidate in Shaanxi Normal University. He interests in plasmonics.

Liang Cao is a B.S. student in Shaanxi Normal University. He interests in plasmonics.

Zhongyue Zhang received the B.Sc. and M.Sc. degrees from Lanzhou University, Lanzhou, China, and the University of Science and Technology of China, Hefei, Anhui, China, in 1994 and 2004, respectively, and the Ph.D. degree from the University of Georgia, Athens, GA, USA, in 2009. He is a Professor at the School of Physics and Information Technology, Shaanxi Normal University. He held Natural Science Foundation of China at Southwest University from 2011 to 2013. He has been working as the Vice President of the research of School of Physics and Information Technology, Shaanxi Normal University since 2013. His research interests include nanophotonics for plasmonic chiral material, optical waveguide material, and broadband extraordinary optical transmission.